

Magnetic breakdown and Landau-level spectra of a tunable double-quantum-well Fermi surface

N. E. Harff,* J. A. Simmons, S. K. Lyo, and J. F. Klem
Sandia National Laboratories, Albuquerque, New Mexico 87185

G. S. Boebinger, L. N. Pfeiffer, and K. W. West
Bell Laboratories, Lucent Technologies, Murray Hill, New Jersey 07974
(Received 9 January 1997; revised manuscript received 25 February 1997)

By measuring longitudinal resistance, we map the Landau-level spectra of double quantum wells as a function of both parallel (B_{\parallel}) and perpendicular (B_{\perp}) magnetic fields. In this continuously tunable highly nonparabolic system, both the cyclotron mass and Fermi energy of the two Fermi surface orbits change in opposite directions with B_{\parallel} . The two corresponding ladders of Landau levels formed at finite B_{\perp} thus exhibit multiple crossings. A third set of Landau levels, independent of B_{\parallel} , arises from magnetic breakdown of the Fermi surface. Semiclassical calculations show good agreement with the data. [S0163-1829(97)51520-7]

Interest in double quantum wells (DQW's) has been growing for several years, owing to the additional degree of electronic freedom available in this system. Phenomena investigated include interlayer tunneling as a function of in-plane (B_{\parallel}) and perpendicular (B_{\perp}) magnetic fields,^{1,2} resistance resonances,³ Coulomb drag,⁴ and a Coulomb-driven correlated bilayer state.⁵⁻⁷ More recently it was shown that at high B_{\parallel} , closely coupled DQW's exhibit an anticrossing in the dispersion curve, leading to additional singularities in the density of states.⁸⁻¹¹ In these experiments, B_{\parallel} shifts the two QW Fermi circles relative to one another in \mathbf{k} space, thereby providing a controlled distortion of the two noncircular orbits of the coupled DQW Fermi surface (FS). B_{\perp} then superimposes Landau-level (LL) structure on this distorted FS. Because the two separate FS orbits have greatly distorted cyclotron masses which depend strongly on B_{\parallel} ,^{12,13} the LL spectrum is expected to be unusually complex. The situation is further complicated by magnetic breakdown,^{14,15} in which an electron tunnels in \mathbf{k} space from one FS orbit to the other. However, while Boebinger *et al.*¹⁶ have observed Fermi circle distortions in DQW's, and Hu and MacDonald¹⁷ have performed a quantum-mechanical calculation for this system which takes into account magnetic breakdown of the FS, to date no one has addressed the issue of LL formation at values of B_{\parallel} large enough to produce the density of states singularities associated with the energy level anticrossing.

In this work, we experimentally map the LL spectrum of two closely coupled GaAs/Al_xGa_{1-x}As DQW structures in tilted fields, by measuring the longitudinal resistance R_{XX} as a function of both B_{\parallel} and B_{\perp} . We observe three separate sets of LLs, corresponding to three different types of FS orbits. (See Fig. 1) The first set arises from the inner, lens-shaped orbit, which has low mass and becomes *less populated* with increasing B_{\parallel} . By contrast, the second set arises from the outer, peanut-shaped orbit, which has high mass and becomes *more populated* with B_{\parallel} . As a result, sweeping B_{\parallel} induces multiple crossings of the LLs at the chemical potential μ . A third set of LLs, insensitive to B_{\parallel} , arises from magnetic breakdown of the FS, whereby electrons tunnel in \mathbf{k} space between the peanut and lens orbits so as to form circular orbits corresponding to separate, uncoupled QW's. A semiclassical calculation of the LL spectrum, taking into

account the B_{\parallel} dependence of both the mass and Fermi energy of each orbit, shows good agreement with the data.

We investigated two modulation-doped GaAs/Al_{0.3}Ga_{0.7}As DQW's, each consisting of two QW's of equal width w separated by a barrier of thickness t . Along with w and t , Table I lists the $B_{\parallel}=0$ values for the electron densities in the two lowest subbands (n_1 and n_2), the total mobility, and the symmetric-antisymmetric energy gap Δ_{SAS} .⁵ [Δ_{SAS} was determined at $B_{\parallel}=0$ from Shubnikov-de Haas (SdH) oscillations as a function of top gate bias.] The QW's are somewhat imbalanced, since $(n_1 - n_2)\pi\hbar^2/m^*$ is somewhat larger than Δ_{SAS} .⁸ Standard four-terminal lock-in measurements were performed. To achieve variation of both B_{\perp} and B_{\parallel} , roughly 900 sweeps of total magnetic field B_T are done with the sample oriented at different angles θ (where $B_{\parallel}=0$ at $\theta=0^\circ$) set by an *in situ* rotating stage. During a sweep, $T=0.3$ K and θ are held constant; between sweeps θ is changed *in situ* at a rate sufficiently slow that T remains below 1 K. B_{\parallel} and B_{\perp} are determined using two identically calibrated Hall probes: one measures B_T , while the other is mounted on the rotating stage so as to measure B_{\perp} only.

The main effect of B_{\parallel} is a linear shift in \mathbf{k} space Δk

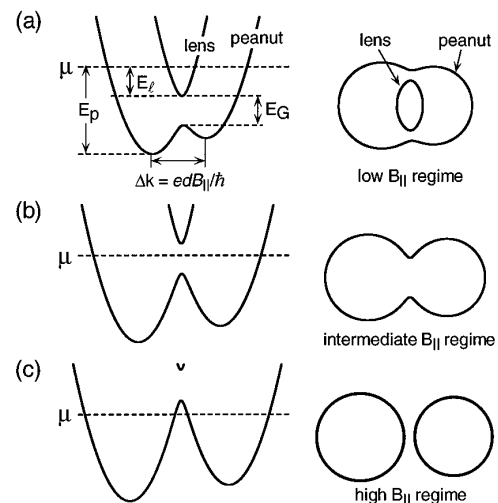


FIG. 1. Sketch of the dispersion (left) and Fermi surface for $\mu \sim 6.8$ meV (right) for sample A at $B_{\parallel} =$ (a) 5.0 T, (b) 7.0 T, and (c) 9.0 T.

TABLE I. Sample parameters.

Sample	w/t (Å)	$n(10^{11} \text{ cm}^{-2})$		μ_{total} ($10^3 \text{ cm}^2/\text{Vs}$)	Δ_{SAS} (meV)
		n_1	n_2		
A	150/15	1.0	1.9	310	2.3
B	139/28	1.9	2.4	740	1.5

$=edB_{\parallel}/\hbar$ of one QW dispersion curve with respect to that of the other, where d is the distance between the two electron layers. When the QW's are strongly coupled, the two QW dispersion curves anticross and a partial energy gap $E_G \approx \Delta_{\text{SAS}}$ appears.^{8,9} Figure 1 shows a sketch of the dispersion curve and FS for sample A in each of three distinct B_{\parallel} regimes. At low B_{\parallel} [Fig. 1(a)] the energy gap is below μ and the FS has two components, an inner lens-shaped orbit, and an outer peanut-shaped orbit. Δk_y increases with B_{\parallel} , causing the gap to move upwards in energy and simultaneously the Fermi energy of the lens orbit E_L to decrease. By contrast, the peanut Fermi energy E_P remains unchanged. At intermediate B_{\parallel} [Fig. 1(b)] μ resides in the gap, and the FS contains only the peanut orbit. Finally, at high B_{\parallel} [Fig. 1(c)] the bottom of the energy gap moves above μ and the FS now consists of two uncoupled circular orbits.

In Fig. 2(a) we plot R_{XX} versus B_{\perp} at a constant $B_{\parallel}=4.5$ T for sample A. At low B_{\perp} , slow SdH oscillations from the lens orbit are apparent, with maxima occurring whenever a LL from the lens crosses μ . As B_{\perp} is increased, additional rapid SdH oscillations from the peanut orbit also appear. At even higher B_{\perp} , the structure becomes more complex, making the origin of individual peaks in R_{XX} difficult to ascertain. In Fig. 2(b) we plot R_{XX} versus B_{\parallel} at a constant $B_{\perp}=0.35$ T, also for sample A. The large oscillations are due to the successive depopulation of lens LLs by an increasing B_{\parallel} . Also evident are smaller, short period oscillations, which by contrast, are due to the successive *population* of LLs in the peanut orbit by B_{\parallel} .

A more complete understanding can be gained from Fig. 3, which shows contour plots of $R_{XX}(B_{\parallel}, B_{\perp})$ for both samples. [Also shown, as thin black lines in 3(a) and 3(b), are the results of a semiclassical calculation to be discussed below.] For sample A [Fig. 3(a)], the data span all three B_{\parallel}

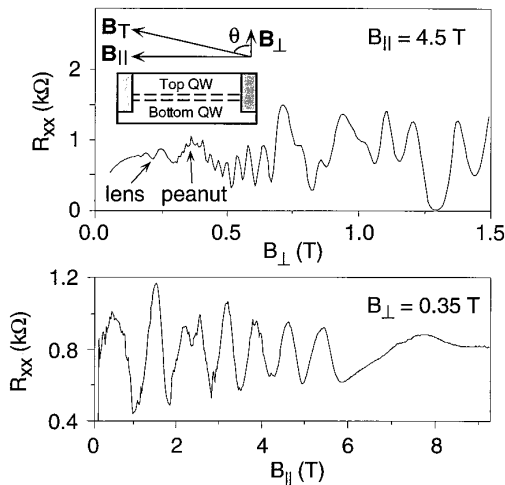


FIG. 2. For sample A, measured (a) $R_{XX}(B_{\perp})$ for fixed $B_{\parallel}=4.5$ T, and (b) $R_{XX}(B_{\parallel})$ for fixed $B_{\perp}=0.35$ T. Inset shows the experimental geometry.

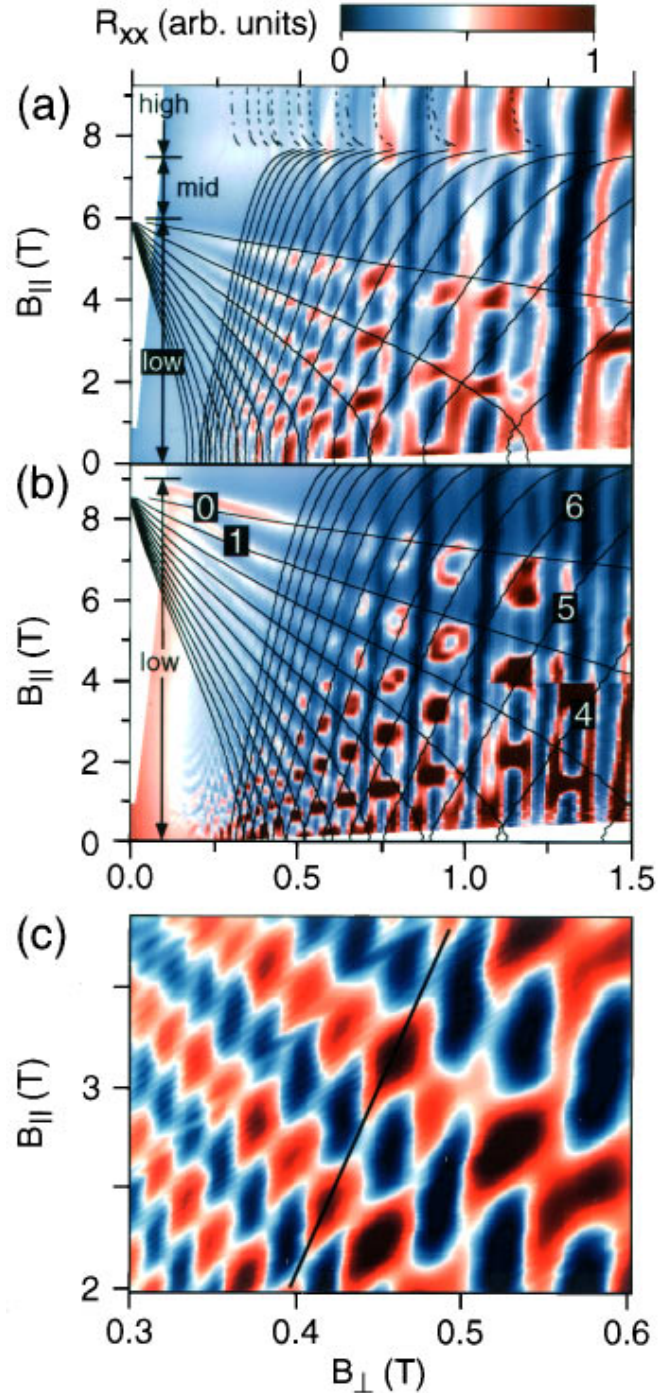


FIG. 3. (Color) Measured $R_{XX}(B_{\parallel}, B_{\perp})$ for (a) sample A, and (b) sample B. Overlaid thin black lines are semiclassically calculated B_{\parallel}, B_{\perp} values at which the lens and peanut LLs (solid), and larger (dashed) and smaller (dash-dotted) QW Fermi circle LLs cross the chemical potential μ . In (b) the $N=0$ and 1 lens and $N=4, 5$, and 6 peanut LLs are labeled. The B_{\parallel} regimes are indicated. (c) Expanded view of the data for sample A, with the R_{XX} range of the color scale halved to enhance the contrast. The black line indicates a single peanut LL.

regimes: high B_{\parallel} (>7.5 T), intermediate B_{\parallel} ($6.0 \text{ T} < B_{\parallel} < 7.5$ T), and low B_{\parallel} (<6.0 T). For sample B [Fig. 3(b)], only the low B_{\parallel} (<9.0 T) and part of the intermediate B_{\parallel} (>9.0 T) regimes are present, because the electron densities n_1 and n_2 are higher. We first discuss the high B_{\parallel} regime. Here oscillations versus B_{\perp} are nearly independent of B_{\parallel} , resulting in a set of vertical high resistance ridges. This is as

expected since the energy gap is above μ ; the FS consists of two well-separated circle orbits [see Fig. 1(c)] whose sizes do not change with B_{\parallel} .

The low B_{\parallel} regime exhibits a more complex R_{XX} which depends strongly on B_{\parallel} . High resistance ridges can clearly be seen running from the upper left towards the lower right, and are due to LLs from the lens orbit coinciding with μ . This clear depopulation of lens LLs with B_{\parallel} is due to two effects. First, as B_{\parallel} is increased, E_{\perp} decreases, roughly as the square of B_{\parallel} .⁸ Second, there is a concurrent increase in the lens LL energy spacing $\hbar\omega_{\perp} = eB_{\perp}/m_p^*$, due to the decrease in m_p^* arising from the distorted dispersion.^{12,13} Also apparent in Fig. 3, most clearly for sample A, is a second weaker set of high resistance ridges running from the lower left towards the upper right. To aid identification of these ridges, Fig. 3(c) shows an expanded view of a region of $R_{XX}(B_{\parallel}, B_{\perp})$ for sample A. These ridges are due to the peanut orbit, which is so large that relatively few electrons can complete it without scattering, accounting for the weakness. (As discussed below, the sharp peaks in R_{XX} occur when the peanut LLs intersect the lens LLs.) In contrast to the lens, the filling factor of the peanut LLs *increases* with B_{\parallel} . While E_p remains nearly constant with B_{\parallel} , the peanut cyclotron mass m_p^* increases,¹³ leading to a decrease in the peanut LL energy separation $\hbar\omega_p = eB_{\perp}/m_p^*$. Finally, a third set of R_{XX} ridges, running vertically, is also apparent. While these vertical ridges are relatively weak at low B_{\perp} , their strength increases rapidly with B_{\perp} so that they dominate R_{XX} at high B_{\perp} . This third set is due to magnetic breakdown, in which electrons tunnel between the lens and peanut orbits so as to form circular orbits corresponding to the individual QW's. The magnetic breakdown is weak at low B_{\perp} , but becomes stronger as B_{\perp} is increased, as expected: larger B_{\perp} causes the electrons to circulate more rapidly around the FS orbits, decreasing the range of each electron's orbit in real space. This reduced uncertainty in the electron position increases the uncertainty in its momentum, thereby enabling tunneling once the \mathbf{k} space uncertainty becomes comparable to the \mathbf{k} -space gap separating the FS orbits.^{14,17}

At intermediate B_{\parallel} , very weak oscillations appear, primarily as nearly vertical ridges. Here μ lies in the energy gap and only the peanut orbit is present. We also attribute these strong vertical ridges to magnetic breakdown, except in this case electrons form circular orbits by tunneling across the neck of the peanut orbit. The peanut orbit produces only slight wiggles in the vertical R_{XX} ridges, occurring whenever a peanut LL crosses a LL due to magnetic breakdown.

Our overall explanation of $R_{XX}(B_{\parallel}, B_{\perp})$ is further supported by Fig. 4, which shows Fourier power spectra of the data in $1/B_{\perp}$ of Figs. 3(a) and 3(b) over the range $0.1 < B_{\perp} < 1.2$ T, for sample A [Fig. 4(a)] and sample B [Fig. 4(b)]. For both samples, a low-frequency peak due to the lens orbit and a high-frequency peak due to the peanut orbit are clearly seen. As B_{\parallel} is increased, the lens (peanut) peak moves to smaller (larger) frequencies, indicating a decreasing (increasing) area in \mathbf{k} space. Two intermediate frequency peaks are also seen due to magnetic breakdown. These peaks remain relatively unchanged with B_{\parallel} .¹⁸ At low B_{\parallel} , sample B exhibits a significant contribution from the QW Fermi circles, due to magnetic breakdown between the lens and peanut orbits.

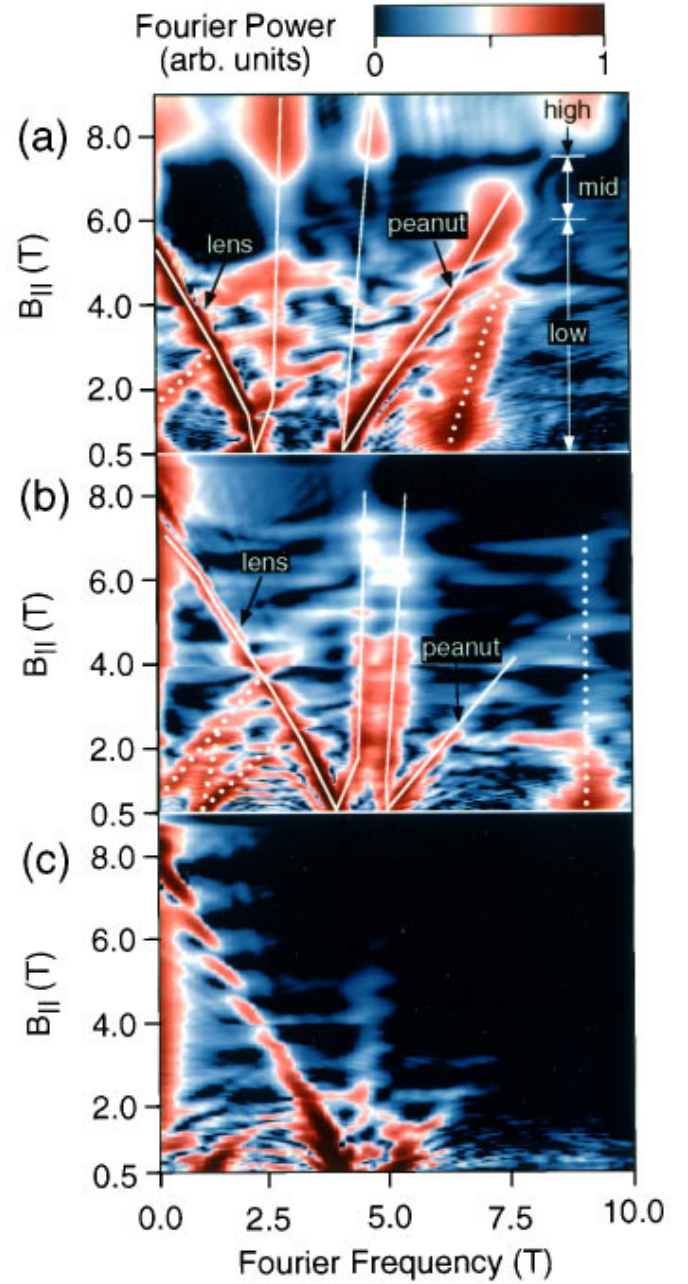


FIG. 4. (Color) Fourier power in $1/B_{\perp}$ of the data of Fig. 3, for (a) sample A, and (b) sample B, for $0.1 < B_{\perp} < 1.2$ T. Overlaid white lines indicate the orbit peaks (solid) and their sum and difference (dotted). The B_{\parallel} regimes are indicated. (c) same as (b), but only for $0.1 < B_{\perp} < 0.5$ T.

Sample A, on the other hand, shows a strong peanut peak but does not as clearly resolve the two QW frequencies until the high B_{\parallel} regime ($B_{\parallel} > 7.5$ T), because its larger Δ_{SAS} inhibits magnetic breakdown.^{14,17} The presence of magnetic breakdown is further illustrated by Fig. 4(c), which shows another contour plot of Fourier power spectra for sample B. However, in this case, the data transformed was only in the range $0.1 < B_{\perp} < 0.5$ T. The relative strength of the intermediate frequency QW peaks is greatly reduced, consistent with magnetic breakdown occurring only at higher B_{\perp} .

At this point it is evident that the data clearly exhibit magnetic breakdown. The individual QW peaks appear not only in the high B_{\parallel} regime where the two Fermi circles are separated, but also in the intermediate and low B_{\parallel} regimes,

where they can occur only if magnetic breakdown is present. In this system, identification of magnetic breakdown is uniquely facilitated by the fact that B_{\parallel} continuously and controllably changes the Fermi surface, moving it from a regime in which breakdown is not possible (high B_{\parallel} and/or $B_{\parallel} \equiv 0$), to a regime in which breakdown occurs via different cusps in the *same* \mathbf{k} -space orbit (intermediate B_{\parallel}), and finally to one in which breakdown occurs via tunneling between *different* \mathbf{k} -space orbits (low B_{\parallel}). By Fourier transforming the data, the identification of each orbit is unambiguously made, and their evolution with B_{\parallel} is readily observed.

To provide a more quantitative test of our model, we perform a simple semiclassical calculation of the B_{\parallel}, B_{\perp} values at which the lens and peanut LLs cross μ . The DQW potential is obtained from the flat-band potential of the growth structures by adjusting the depth of each QW so as to obtain the measured values of the uncoupled densities. An equal but opposite amount of linear band bending is then artificially added to each QW so as to yield the measured Δ_{SAS} value. (A Hartree calculation gives only minor differences in the calculation results.) The DQW potential thus obtained is then used to find the uncoupled QW wave functions and eigenvalues, which are then used in a tight-binding calculation of the DQW dispersion $E(k_x, k_y, B_{\parallel})$ following Lyo.^{8,13} From $E(k_x, k_y, B_{\parallel})$ we obtain $E_{\ell/p}(B_{\parallel})$, making the approximation that $E_p(B_{\parallel})$ and μ are constant. (While this approximation seems poor when only the peanut is occupied at intermediate B_{\parallel} , the presence of strong magnetic breakdown makes it more reasonable, since the QW LLs provide a reservoir of electrons.) The tight-binding calculation also yields the cyclotron masses $m_{\ell/p}^*(B_{\parallel}) = (\hbar^2/2\pi) \partial A_{\ell/p} / \partial E$, where $A_{\ell/p}$ is the area in \mathbf{k} space of the (lens or peanut) orbit evaluated at μ . The LL energies are then given by $E_{\ell/p} = (N_{\ell/p} + 1/2)\hbar e B_{\perp} / m_{\ell/p}^*(B_{\parallel})$, where the LL index $N_{\ell/p} = 0, 1, 2, \dots$, and spin splitting is ignored. This approach makes the simplifying approximation that each energy branch is well described by a constant $m_{\ell/p}^*$ for each B_{\parallel} . The B_{\parallel}, B_{\perp} values at which the LLs cross μ are then obtained by fixing $N_{\ell/p}$ and B_{\parallel} , and finding the B_{\perp} which makes this relation an equality. We make the further simplifying approximation that $E_{\ell/p}$ is constant with B_{\perp} .

The results of this calculation are shown as thin black lines in Figs. 3(a) and 3(b). All the essential features of the experimental data, in particular the approximate positions of the lens and peanut LLs, are reproduced. The sharp R_{XX} peaks in the data correspond closely with the calculated intersection points of the lens and peanut LLs.¹⁹ The calculation also recreates the wiggles in the vertical R_{XX} ridges in the intermediate B_{\parallel} regime, due to peanut LLs crossing magnetic breakdown LLs. The calculation's unusual behavior near $B_{\parallel} = 7.5$ T for sample A is due to the saddle point in the peanut dispersion branch, where m_p^* diverges logarithmically.¹³ This leads to a distinctly higher R_{XX} (Ref. 9).

We also performed a full quantum-mechanical calculation of the density of states at μ , diagonalizing the tight-binding Hamiltonian of Hu and MacDonald.¹⁷ This Hamiltonian consists of diagonal elements which represent the Landau ladders of the two QW's displaced by the difference in their subband energies, and inter-ladder (i.e., inter-QW) off-diagonal elements which couple any two rungs of the ladders. Although not shown here, the salient features of the data for both samples are reproduced, with large peaks in the DOS occurring whenever LLs from each FS branch overlap at μ . More details will be presented elsewhere.²⁰

In summary, we have mapped the LL spectra in tilted magnetic fields of two closely coupled DQW's by measuring $R_{XX}(B_{\parallel}, B_{\perp})$. We observe three separate sets of LLs in this tunable, highly nonparabolic system, corresponding to three different types of FS orbits. LLs from the low-mass upper dispersion branch (the lens orbit) become depopulated with increasing B_{\parallel} , while those from the high-mass lower dispersion branch (the peanut orbit) become more populated, causing multiple crossings of the LLs. A third set of LLs, insensitive to B_{\parallel} , arises from magnetic breakdown of the Fermi surface. A semiclassical calculation taking into account the B_{\parallel} dependence of the masses and Fermi energies qualitatively reproduces the data, as does a full quantum mechanical calculation.

Sandia is a multiprogram laboratory operated by Sandia Corporation, a Lockheed-Martin company, for the U.S. Department of Energy under Contract No. DE-AC04-94AL85000.

* Also at Oregon State University, Corvallis, OR.

¹J. P. Eisenstein, *et al.*, Phys. Rev. B **44**, 6511 (1991); J. A. Simmons *et al.*, *ibid.* **47**, 15 741 (1993).

²J. P. Eisenstein *et al.*, Phys. Rev. Lett. **69**, 3804 (1992); K. M. Brown *et al.*, Phys. Rev. B **50**, 15 465 (1994).

³A. Palevski *et al.*, Phys. Rev. Lett. **65**, 1929 (1990).

⁴T. J. Gramila *et al.*, Phys. Rev. Lett. **66**, 1216 (1991).

⁵G. S. Boebinger, *et al.*, Phys. Rev. B **45**, 11 391 (1992).

⁶A. H. MacDonald, P. M. Platzman, and G. S. Boebinger, Phys. Rev. Lett. **65**, 775 (1990).

⁷S. Q. Murphy *et al.*, Phys. Rev. Lett. **72**, 728 (1994).

⁸S. K. Lyo, Phys. Rev. B **50**, 4965 (1994).

⁹J. A. Simmons *et al.*, Phys. Rev. Lett. **73**, 2256 (1994).

¹⁰A. Kurobe *et al.*, Phys. Rev. B **50**, 4889 (1994); F. T. Vasko and O. E. Raichev, *ibid.* **23**, 16 349 (1995).

¹¹T. S. Lay, *et al.*, Phys. Rev. B **52**, R5511 (1995).

¹²N. E. Harff *et al.*, in *Proceedings of the 22nd International Conference on Physics of Semiconductors, Vancouver, 1994*, edited by D. J. Lockwood (World Scientific, Singapore, 1995), p. 831; J. A. Simmons, N. E. Harff, and J. F. Klem, Phys. Rev. B **51**, 11 156 (1995).

¹³S. K. Lyo, Phys. Rev. B **51**, 11 160 (1995).

¹⁴E. I. Blount, Phys. Rev. **126**, 1636 (1961); N. W. Ashcroft and N. D. Mermin, *Solid State Physics* (Saunders College, Philadelphia, 1976), p. 774.

¹⁵N. E. Harff *et al.*, in *Proceedings of the 23rd International Conference on Physics of Semiconductors, Berlin, 1996*, edited by M. Scheffler and R. Zimmerman (World Scientific, Singapore, 1996), p. 2199; and N. E. Harff *et al.*, *Superlattices and Microstructures* **20**, 595 (1996).

¹⁶G. S. Boebinger *et al.*, Phys. Rev. B **43**, 12 673 (1991).

¹⁷J. Hu and A. H. MacDonald, Phys. Rev. B **46**, 12 554 (1992).

¹⁸At very low B_{\parallel} the QW peaks change position because Δ_{SAS} begins to contribute to the difference in subband energies (see Refs. 8 and 13). In addition, a small drift to higher frequency with B_{\parallel} occurs due to a distortion in the shape of the individual QW Fermi circles. See L. Smrcka *et al.*, Phys. Rev. B **51**, 18 011 (1995).

¹⁹While the peaks in the data appear to form rows that do not coincide with the calculated LLs, this is an illusion caused by the close spacing of the intersection points. The alternating strength of these rows, most evident for sample B around 0.2 T < B_{\perp} < 0.6 T, is in fact due to a beating of the intersection points with the magnetic breakdown LLs.

²⁰S. K. Lyo (unpublished).